Controlled Evaluation of Silver Nanoparticle Dissolution Using Atomic Force Microscopy

ARTICLE *in* ENVIRONMENTAL SCIENCE & TECHNOLOGY · DECEMBER 2011

Impact Factor: 5.33 · DOI: 10.1021/es203475a · Source: PubMed

Environmental Science & Technology

Article

pubs.acs.org/est

Controlled Evaluation of Silver Nanoparticle Dissolution Using Atomic Force Microscopy

Ronald D. Kent and Peter J. Vikesland*

Department of Civil and Environmental Engineering, Institute of Critical Technology and Applied Science (ICTAS), and the Center for the Environmental Implications of Nanotechnology (CEINT), Virginia Tech, 418 Durham Hall, Blacksburg, Virginia 24060-0246, United States

Supporting Information

ABSTRACT: Incorporation of silver nanoparticles (AgNPs) into an increasing number of consumer products has led to concern over the potential ecological impacts of their unintended release to the environment. Dissolution is an important environmental transformation that affects the form and concentration of AgNPs in natural waters; however, studies on AgNP dissolution kinetics are complicated by nanoparticle aggregation. Herein, nanosphere lithography (NSL) was used to fabricate uniform arrays of AgNPs immobilized on glass substrates. Nanoparticle immobilization enabled controlled evaluation of AgNP dissolution in an air-saturated phosphate buffer (pH 7.0, 25 °C) under variable NaCl concentrations in the absence of aggregation. Atomic force microscopy (AFM) was used to monitor changes in particle morphology and dissolution. Over the first day of exposure to ≥10 mM NaCl, the in-plane AgNP shape changed from triangular to circular, the sidewalls steepened, the in-plane radius decreased by 5−11 nm, and the height increased by 6−12 nm. Subsequently, particle height and in-plane radius decreased at a constant rate over a 2-week period. Dissolution rates varied linearly from 0.4 to 2.2 nm/d over the 10−550 mM NaCl concentration range tested. NaCl-catalyzed dissolution of AgNPs may play an important role in AgNP fate in saline waters and biological media. This study demonstrates the utility of NSL and AFM for the direct investigation of unaggregated AgNP dissolution.

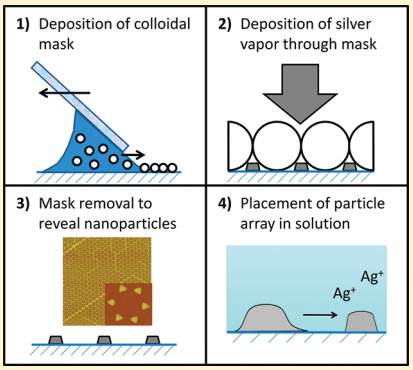

INTRODUCTION

As a result of their biocidal properties, silver nanoparticles (AgNPs) have been incorporated into a wide range of consumer products, including textiles, plastics, cosmetics, household sprays, and paints with the total number of applications rapidly increasing.[1−3] There is significant potential for release of AgNPs from these products into the environment,[2,4,5] and this discharge into aquatic systems could have unintended detrimental ecological impacts.[1]

AgNP toxicity has been demonstrated for several species of vertebrates, invertebrates, and prokaryotic and eukaryotic microorganisms, as well as some mammalian cell lines and viruses.[1,6] Studies have shown that size,[7−9] shape,[10] surface coating,[11,12] and solution chemistry[13,14] all influence AgNP toxicity. The toxicity of the free silver ion, Ag^+, and its complexes has been well documented, but there is ongoing debate over whether the observed toxicity of AgNPs is due to the release of Ag^+ alone, or if the nanoparticles themselves exert a direct toxic effect.[14−16] Some researchers have suggested that AgNPs are similar to a drug delivery system in which the AgNPs transport and deliver biologically active Ag^+ to a biological target.[17] Under this paradigm, the biological activity of AgNPs is controlled by Ag^+ release rates, which, in turn, are controlled by size, shape, surface coating, and so forth.[17]

Even if Ag^+ is only partially responsible for the observed toxic effects of AgNPs, dissolution may still be an important environmental transformation that dictates the concentration and form of silver to which aquatic organisms are exposed. For this reason, several studies have explored the dissolution kinetics of AgNPs under a variety of conditions;[17−21] however, particle aggregation was uncontrolled in each of these studies and the potential effects of aggregation on nanoparticle dissolution rates were given little to no attention. Recently, however, studies performed with magnetite[22] and galena[23] nanoparticles, goethite nanorods,[24] and nC_{60} suspensions[25,26] have demonstrated that aggregation decreases nanomaterial reactivity by an order of magnitude or more. This decreased reactivity is explained in part by diminished particle surface area in contact with the solution phase and hindered mass transport to reactive sites within dense aggregate structures.[22,23]

The objective of this work was to use nanosphere lithography (NSL) to fabricate uniform arrays of AgNPs immobilized on glass substrates to enable the evaluation of AgNP dissolution under highly controlled conditions in the absence of aggregation. NSL was chosen because it is a versatile, inexpensive, and high-throughput lithographic technique that

Special Issue: Transformations of Nanoparticles in the Environment

Received: September 30, 2011
Revised: December 9, 2011
Accepted: December 15, 2011

   dx.doi.org/10.1021/es203475a | Environ. Sci. Technol. XXXX, XXX, XXX−XXX

enables creation of periodic nano- and microparticle arrays.[27] NSL facilitates control over size, shape, and interparticle spacing for a number of different materials and substrates.[28−31] In this study, the dissolution rates of NSL-produced AgNPs were quantified by atomic force microscopy (AFM), which gave a detailed description of changes in particle size and shape as a function of time and NaCl concentration. This work demonstrates the utility of NSL for future studies examining nanomaterial fate in the environment.

MATERIALS AND METHODS

Dissolution experiments were conducted in phosphate buffers produced by dissolving 1 mM NaH_2PO_4 and 1 mM Na_2HPO_4 in air-saturated deionized (DI) water (18.2 MΩ cm, Barnstead). Aliquots of 5 M NaCl were added to the buffer to achieve variable NaCl concentrations (10−550 mM) and the solution pH was adjusted to 7.0 ± 0.1 using 0.1 N NaOH. The highest NaCl concentration used is characteristic of seawater, while the lowest is approximately representative of cytoplasm.[17] All dissolution experiments were conducted at room temperature (25 °C) in the dark. Glass substrates (60 × 24 × 0.15 mm microscope cover glass, Fisher Scientific) were cleaned by immersion in a solution of 4% NH_4OH/16% H_2O_2 at 75 °C for 10 min, followed by an additional 10 min in 14% HCl/14% H_2O_2 at 75 °C. The substrates were rinsed thoroughly with DI water after each cleaning step and dried using filtered air after the final rinse. Glassware used for substrate production was cleaned similarly, and glassware used for acid digestion was cleaned by soaking overnight in 14% HNO_3 and was then rinsed with DI water.

Substrate Production. After cleaning, the glass substrates were thiolated by immersing them in 5% (3-mercaptopropyl)-trimethoxysilane (Sigma-Aldrich) dissolved in spectrophotometric grade methanol (Alfa Aesar) overnight.[32] Thiol groups have a strong affinity for soft metals such as silver, and preliminary experiments indicated that the AgNPs were highly mobile on the substrate if the glass was not thiolated prior to use. Following thiolation, glass substrates were rinsed with and stored in methanol until use.

Convective self-assembly (CSA), as described by Chen et al.,[33] was used to deposit a monolayer of 450-nm diameter carboxylated latex spheres (4% w/v, Invitrogen) onto the thiolated substrates. Briefly, the substrates were held horizontally on a motion stage (Thor Laboratories) approximately 10−200 μm below an angled plate. This CSA assembly was enclosed in an airtight container. Prior to surface application, centrifugation was used to concentrate the latex colloid suspension 5-fold. A drop of this concentrated latex colloid suspension was placed between the substrate and the angled plate. The substrate was then moved at a constant velocity relative to the plate, causing the colloidal suspension to be spread over the substrate. Solvent evaporation induced the latex spheres to crystallize into a hexagonally close-packed monolayer.

Following CSA, silver metal was vacuum deposited onto the substrates by electron beam evaporation (3-kW electron gun, Thermionics).[34] Prepared substrates were stored in sealed glass jars for periods up to several months until use. Immediately prior to use, substrates were cut into approximate 2 × 2 mm specimens and attached to 15-mm AFM specimen discs (Ted Pella) using wax. The latex spheres were then removed by sonication in ethanol for 1 min. Each specimen was rinsed in DI water for 1 min and dried with filtered air. ImageJ (NIH) was used to estimate the total area of each specimen based upon digital images.

The total amount of silver deposited was determined for five prepared specimens by placing each sample in 10 mL of 5% trace metal grade HNO_3 (Fisher Scientific)/3% H_2O_2 at 120 °C on a hot plate for 1 h followed by analysis of the supernatant via inductively coupled plasma-mass spectrometry (ICP-MS, Agilent 7500C). A brief discussion of this digestion procedure is included in the Supporting Information (SI). The solution volume was restored to 10 mL using DI water prior to ICP-MS analysis. A LEO (Zeiss) 1550 Schottky field-emission scanning electron microscope (SEM) equipped with an Oxford INCA Energy E2H X-ray energy dispersive spectrometer (EDS) system with silicon drift detector was used for SEM and EDS measurements. Samples were sputter coated with gold−palladium for 30 s prior to SEM imaging. SEM images were analyzed using ImageJ. X-ray photoelectron spectroscopy (XPS) was performed using a PHI Quantera XPS microprobe.

Nanoparticle Dissolution Experiments. After initial characterization by AFM, prepared specimens were submerged in 10-mL aqueous samples of variable NaCl concentrations in 15-mL polystyrene sample tubes (Fisher Scientific), sealed, and then placed in the dark. Each specimen was periodically removed from solution for AFM characterization. Upon completion of the predetermined incubation period, the supernatant was acidified with 200 μL of 67−70% HNO_3 and analyzed by ICP-MS to determine the dissolved silver concentration.

A Nanoscope IIIa Multimode AFM (Digital Instruments) equipped with a J scanner and silicon probes (TESP, spring constant of 20−80 N/m, Bruker) was used to obtain all AFM data. All images were collected in tapping mode in air using a 256 × 256 pixel resolution at a scan rate of 0.5−1.0 Hz. Mean particle heights and radii were determined from 5 × 5 μm and 3 × 3 μm AFM images, where radius is defined as the radius of a circle of equivalent area, as described in the SI. The average number of particles measured to determine the mean particle height and radius at each time point was 142 with a minimum number of 42. High-resolution AFM images (300 × 300 nm) were used for numerical volume integrations and the deconvolution procedure described below. The "Particle Analysis" extension of the NanoScope software was used with a threshold height of 10 nm for analysis of AFM data. Irregular particles resulting from defects in the latex colloid mask were excluded from analysis.

Data Analysis. A deconvolution algorithm developed by Markiewicz and Goh[35] was performed to estimate the correction factors used to account for distortions in lateral particle dimensions by the AFM probe. In essence, the algorithm places a facsimile of the known or assumed AFM probe shape, in this case a spherical tip with an 8-nm radius, at each data point and compares the geometry of the probe with the surrounding data points. Data points that conflict with the probe geometry have their height decreased to the highest point at which there is no conflict. Based on results from this technique, a radius correction factor of 6 nm was estimated for the initial time point, and a correction factor of 7 nm was used for subsequent time points in all instances except for the case where no NaCl was added to the phosphate buffer; under the latter conditions no significant change in the particle radius was observed by AFM during the time frame of the experiment.

To convert AFM mean height and corrected mean radius measurements to average particle volumes, a mathematical

dx.doi.org/10.1021/es203475a | Environ. Sci. Technol. XXXX, XXX, XXX−XXX

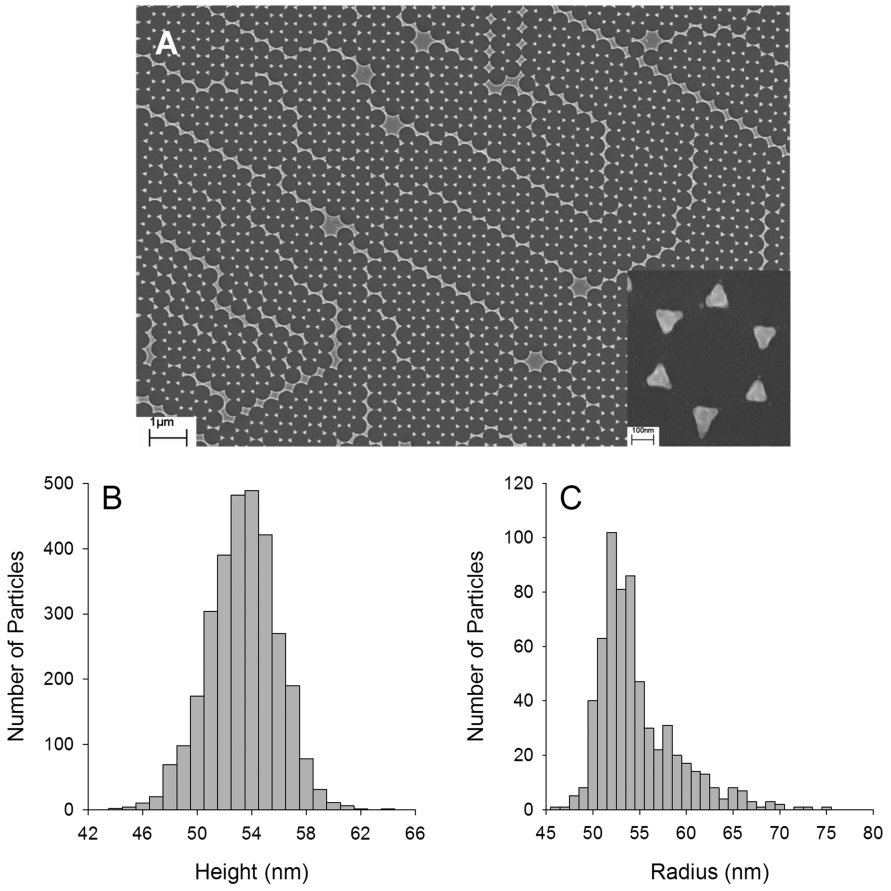

Figure 1. (A) SEM micrograph of a typical NSL-produced AgNP array. (B) Height (N = 3051) and (C) radius (N = 620) distributions measured by AFM and SEM, respectively, for the AgNP arrays used in this study.

description of the corroded particle shape was formulated. High-resolution AFM images of individual AgNPs were deconvoluted according to the method described in the preceding paragraph and then a numerical integration was performed to estimate the volume of individual particles. Several geometric shapes were assumed, using particle height and corrected radius as shape descriptors, and their volumes were compared with the integrated volumes. Additional details on this procedure are included in the SI. The shape whose calculated volume most closely predicted the integrated volumes is described by eq 1.

$$y = h\left[1 - \left(\frac{x}{r}\right)^6\right] \tag{1}$$

where h is the measured particle height (nm), r is the corrected particle radius (nm), x is the horizontal distance from the particle center (nm), and y (nm) is the particle height as a function of x. Equation 1 is defined for $0 \leq x \leq r$, and the 3-dimensional shape is obtained by revolving this function 2π radians about the y-axis. Equation 2 was determined by integration and gives the volume, V_p (nm^3), of the particle described by eq 1.

$$V_p = \frac{3\pi}{4} hr^2 \tag{2}$$

Changes in average particle volume between time points were converted into a predicted aqueous silver concentration, C (μg/L ~ ppb), using eq 3.

$$C = \frac{\rho(\Delta V_p)NA}{V_s} \tag{3}$$

where ρ is the density of bulk silver (1.05×10^{-14} μg/nm^3), N is the number of particles per unit substrate area assuming that the substrates are completely homogeneous (10 particles/μm^2), A is the total area of the specimen (μm^2), and V_s is the solution volume (0.01 L). We emphasize that given that the substrates produced by CSA are not homogeneous, the predicted concentration of silver in suspension obtained using eq 3 is a highly conservative estimate, as discussed fully in the Results and Discussion.

RESULTS AND DISCUSSION

Substrate Characterization. A representative SEM micrograph of a finished AgNP array is shown in Figure 1a. Defect-free domains spanned several μm^2 and both point and line defects are evident. Initial characterization by AFM revealed that the NSL-produced AgNPs had a truncated tetrahedral shape as expected based upon past reports.[27−30] The nanoparticle heights were normally distributed with a mean value of 53.4 ± 0.1 nm (95% confidence) and a standard deviation (SD) of 2.5 nm (Figure 1b). AFM measurements, corrected as detailed in the Materials and Methods, gave a mean particle radius of 56.0 ± 0.1 nm, which qualitatively agrees with the mean radius of 55.0 ± 0.3 nm determined by SEM. The particle radius distribution was positively skewed with SD = 4.3 nm (Figure 1c). Numerical integration of high-resolution AFM data yielded an average volume of 3.1×10^5

dx.doi.org/10.1021/es203475a | Environ. Sci. Technol. XXXX, XXX, XXX−XXX

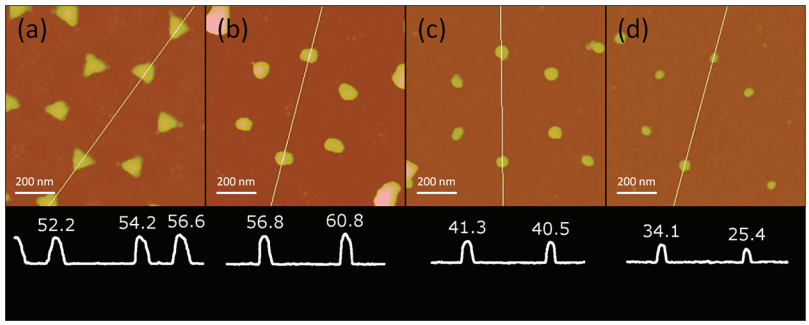

Figure 2. Deconvoluted AFM micrographs and height profiles for NSL-produced AgNP arrays (a) prior to initiation of a dissolution experiment and after (b) 1 d, (c) 7 d, and (d) 15 d of immersion in a 550 mM NaCl phosphate buffer at pH 7.0 and 25 °C. Labeled particle heights are in units of nm. The four images were acquired at four different locations.

nm^3/particle, which leads to a predicted silver mass for a hypothetical completely homogeneous substrate of 33 mg/m^2. The average total silver determined by ICP-MS was 106 mg/m^2 (SD = 24 mg/m^2). As expected, the value measured by ICP-MS was higher than the value predicted for a homogeneous substrate since the defects shown in Figure 1a contribute more mass per unit area than the individual particles. Numerous attempts to produce defect free substrates were unsuccessful—presumably due to surface heterogeneities in the glass substrates.

Change in Silver Nanoparticle Shape. During the first day of exposure to solutions of ≥10 mM NaCl, AFM measurements indicated that the in-plane AgNP shape changed from triangular to circular, the sidewalls steepened, and the height increased by 6−12 nm (Figure 2). Similar changes were observed for 1 mM NaCl, but the particles maintained their triangular in-plane shape. Particle radii, as measured by SEM in a separate exposure, decreased by 5−11 nm during the same time period. The decrease in mean radius was only 1−8 nm when measured by AFM. The ∼4 nm discrepancy is probably due to the pixelation of AFM images, which results in less accurate estimates of particle radii by the Particle Analysis software package as features become steeper (see SI for further discussion of AFM lateral dimension resolution issues). Changes in AgNP shape induced by chloride are often ascribed to a dissolution−recrystallization mechanism;[36,37] however, previous studies invariably involve a reductant and a surfactant, so these previous results are not directly comparable to those presented here and several other explanations had to be considered. SEM images (Figure S3) indicated that highly irregular aggregates formed in NaCl solutions to some extent in spite of the thiolation procedure; however, these aggregates were entirely excluded from the AFM analysis, so an aggregation-based mechanism was immediately rejected.

Equilibrium calculations were performed using Visual MINTEQ 2.53 to evaluate the potential for precipitate formation since AgCl precipitation could explain the observed height change and affect the dissolution rates by passivation.[38] AgCl was the least soluble phase (compared with Ag_3PO_4 and Ag_2CO_3) even at high Cl^- concentrations, with the solubility ranging from 80 to 3100 ppb Ag^+ as Cl^- increased from 10 to 550 mM. According to the total silver measurements by ICP-MS, complete dissolution from a 4 mm^2 substrate would result in ∼40 ppb Ag^+, which is even lower than the predicted minimum AgCl solubility of ∼60 ppb Ag^+ at 3 mM Cl^-. The actual amount of silver released was <40 ppb for the duration of all experiments and was lowest in the samples where NaCl concentration was lowest (e.g., 1−3 ppb Ag^+ after 2 weeks of dissolution in 10 mM NaCl−ICP-MS measurements are discussed in the following section), so the Ag^+ concentration was 1 order of magnitude or more below the theoretical solubility threshold of AgCl under each condition. These equilibrium calculations are valid for the bulk solution, but they do not account for the complex chemistry at the nanoparticles' surfaces or possible concentration gradients near the 2-dimensional particle array; therefore, XPS was used as a surface-sensitive technique to probe the substrate for AgCl in three samples where a 4−7 nm height increase was observed. Although silver was readily detected in each case, the Cl 2p and Cl 2s peaks near 200 and 270 eV, respectively, were not present in any of the XPS spectra indicating that an AgCl precipitate was not present (Figure S5). EDS measurements were also performed, but the Cl K_α and K_β peaks near 2.6 and 2.8 keV were not detected (data not shown). Based on this evidence, we conclude that the measured change in height was not due to precipitation. Because predicted environmental AgNP concentrations are even lower than the concentrations used in this study, this conclusion suggests that a layer of AgCl will not form on AgNPs in most natural environments.[39,40]

Upon careful examination of the literature, a hypothesis was qualitatively formulated that involves a redox potential gradient within each individual NSL-produced AgNP. Zhang et al. reported that NSL-produced AgNPs dissolve at the bottom edges first, then at the triangular corners, and finally at the out-of-plane height during electrochemical processing.[41] They attributed this result to the sharp radius of curvature along the particles' bottom edges and corners. Surface free energy contributes substantially to the total free energy for features that exhibit sharp radii of curvature, and this excess surface energy can lead to a more negative redox potential at these sites.[42,43] If regions of a nanoparticle surface with sharp radii of curvature have lower redox potentials than regions with large radii of curvature, then a redox potential gradient must exist between these regions. Ag^+ is known to exist on AgNP surfaces in air-saturated water,[12,18] and we hypothesize that oxidation of Ag^0 to Ag^+ occurred at the bottom edges and corners of the AgNPs (the anode), while reduction of Ag^+ to Ag^0 occurred at their tops (the cathode). This process formed an Ag^+ concentration gradient that favored a net flow of silver from the bottom of a nanoparticle to the top until the internal redox potential gradient was eliminated. Electron transport through the AgNP itself is necessary for a height increase to occur by this mechanism; therefore, such a height increase would not be expected if the electrons were transferred through an electrode,

dx.doi.org/10.1021/es203475a | Environ. Sci. Technol. XXXX, XXX, XXX−XXX

as was done in the work by Zhang et al.[41] This hypothesis is consistent with the observed initial increase in AgNP height with a concomitant steepening of the sidewalls and dissolution at the corners. A similar mechanism has been proposed to explain the simultaneous dissolution of edges and growth of the (001) basal plane of hematite crystals.[44]

This process was most apparent in NaCl solutions and only a small but significant ($\alpha < 0.05$) increase in height occurred in the phosphate buffer alone, thus suggesting a catalytic or reactive role for NaCl. Chloride has been observed in our study and others to catalyze oxidation of AgNPs.[36,37,45,46] Because adsorbed Ag^+ inhibits AgNP oxidation, Cl^- could accelerate silver redox reactions by complexation and removal of Ag^+ from AgNP surfaces.[45] This hypothesis is in agreement with the decrease in particle radius, which was greatest at high NaCl concentrations, but it is inconsistent with our proposed mechanism for the increase in height, which requires adsorption of Ag^+. Indeed, Ag^+ reportedly increases the rate of electrochemical Ostwald ripening of AgNPs, which has a driving force similar to what we have proposed here.[43] Consistent with this view, the height increase was lowest at high NaCl concentrations, possibly because Cl^- effectively held Ag^+ in solution and prevented its adsorption and subsequent reduction to Ag^0 at the top of AgNPs. Because the smallest height increase and greatest radius decrease occurred in 550 mM NaCl, oxidation of the bottom edges and corners by oxygen may have become more important and the internal redox differential of these AgNPs less important at high NaCl concentrations.

An alternate explanation for the catalytic role of Cl^- is the "pre-oxidation" or "pre-complexation" mechanism proposed by Henglein and co-workers.[47,48] They postulated that nucleophiles coordinated to an AgNP surface would force excess negative charge into the AgNP interior; thus, chloride apparently helps overcome the energy barrier to oxidation by promoting electron transfer through the AgNP interior. According to this hypothesis, the nucleophilic thiols on the glass substrate could potentially have an effect similar to chloride, but their influence seems to be small since only a minimal height change was observed in the buffer alone. Perhaps the inaccessibility of the substrate−silver interface to the solution phase prevented the thiol groups from affecting AgNP oxidation to the same extent as chloride. Additional experimentation, which was outside the scope of the present effort focused on nanoparticle dissolution, is required to fully evaluate the hypothesis that internal redox potential gradients were responsible for the initial change in height. As most manufactured nanoparticles are quasi-spherical, this behavior is not expected to be typical of AgNPs released into the environment.

Dissolution Rates. After the first day, both the mean particle height and radius decreased linearly with time (Figure 3). The dissolution rates (i.e., the slopes of the linear regressions) were significant ($p < 0.001$ for height analyses and $p < 0.05$ for radii analyses) for all the data shown except for the case where no NaCl was added. As shown in Figure 3c, there is a strong linear correlation between the AgNP dissolution rate and the concentration of NaCl ($R^2 = 0.999$) and the measured dissolution rates were the same, within error, for both particle height and radius measurements. Empirical formulas for predicting AgNP dissolution rates as a function of NaCl concentration in units of nm/d and mg/m^2/d are included in the SI, but the applicability of these formulas is limited to the experimental conditions of this study (e.g., pH 7.0, 25 °C, phosphate buffer). If the regression lines are extrapolated to the low NaCl concentrations expected in freshwater (0.1−1 mM), then the effect of NaCl is minimal (i.e., the dissolution rate is predicted to increase by only 0.03 nm/d over the range of 0−10 mM NaCl). On the other hand, the dissolution rate is predicted to increase nearly 6× at NaCl concentrations typical of seawater (i.e., 2.2 nm/d for 550 mM NaCl compared with ∼0.4 nm/d for ≤10 mM NaCl).

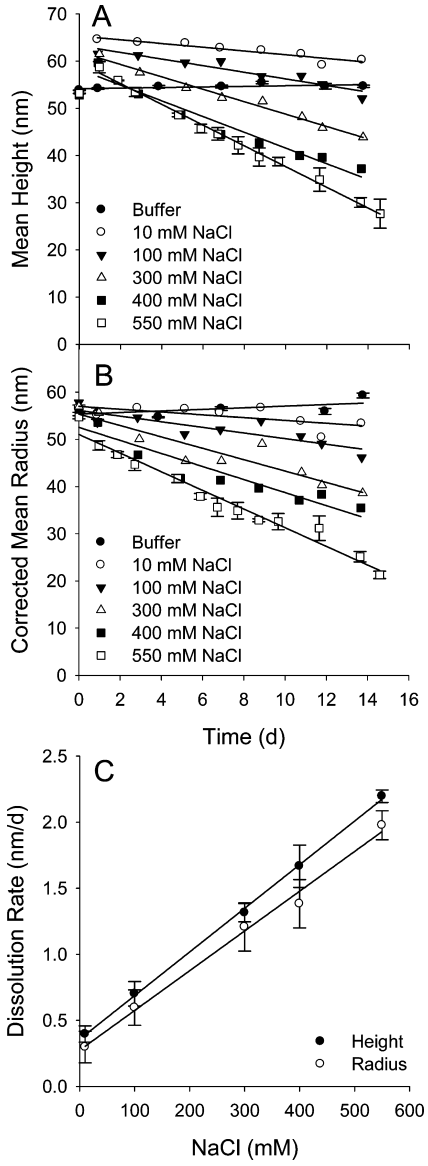

Figure 3. Results of AFM measurements for AgNP dissolution experiments. Variation of mean AgNP (A) height and (B) radius with time at different NaCl concentrations. Error bars, where shown, represent the standard deviation between mean heights or radii determined by AFM for experiments performed in triplicate. Three mean radius measurements were excluded because assumptions about the tip shape were obviously violated. (C) Slopes of the regression lines for AgNP height and radius as a function of NaCl concentration. Standard errors are indicated by the error bars.

Because hydrogen ions and oxygen are consumed during the dissolution reaction, changes in pH and the dissolved oxygen concentration can influence the observed dissolution rates.[18,19] Because the solutions used in this study were air saturated

dx.doi.org/10.1021/es203475a | Environ. Sci. Technol. XXXX, XXX, XXX−XXX

(0.20−0.26 mM O_2), the dissolved oxygen levels were approximately 3 orders of magnitude larger than the highest silver concentration (~0.0003 mM Ag^+); therefore, the dissolved oxygen concentration can be considered constant. Furthermore, the pH of the solutions was well buffered, with the pH in three 550 mM NaCl solutions stable at 7.0 ± 0.1 at the end of a 2-week dissolution period.

By using the regression equations from Figure 3 in conjunction with eqs 2 and 3, the dissolved silver concentration was calculated as a function of time and compared with ICP-MS measurements. Check standards indicated that the NaCl matrix caused the ICP-MS analysis to underestimate the actual silver concentration by as much as 40%. Ionization suppression and salt deposition are known to cause interference with ICP-MS measurements in high-salt matrices.[49] Dilution could not be used to resolve this issue because the Ag^+ concentrations were too low. Discrepancies still occurred after making corrections using internal standards, and no simple calibration could resolve the problem because the error increased with time. Despite the low recoveries, the predicted values were of the same order of magnitude as the actual silver concentrations assuming that the raw measured value and the measured value after adjustment for a 40% error are the lower and upper bounds, respectively (Figure 4). The predicted silver concentration was clearly lower than the real values for NaCl concentrations of 400 and 550 mM because the calculation underestimates the total silver available for dissolution, as noted previously. Thus, the ICP-MS analysis, while not truly quantitative, agrees with the AFM results. Interestingly, Ag^+ clearly went into solution rather than forming complexes with the free thiol groups on the substrate. It is possible that atmospheric oxygen oxidized the free thiols to a form with lower affinity for silver during the storage period of several months. This hypothesis could also explain why the thiol layer did not entirely prevent aggregation upon exposure to NaCl.

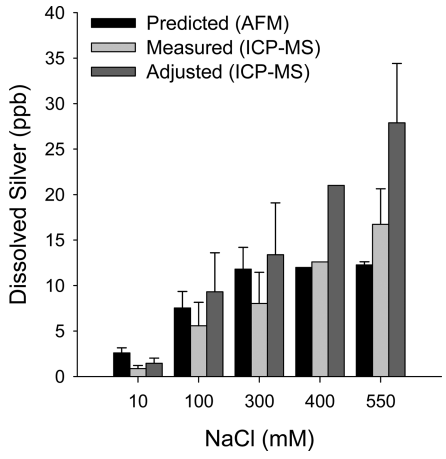

Figure 4. Predicted and measured dissolved silver in solutions of varying NaCl concentrations after approximately 2 weeks of NSL-produced AgNP dissolution. The predicted values are based on linear regression of AFM data (Figure 3) in conjunction with eqs 2 and 3. ICP-MS was used for the measured values, but quality controls indicated that the measured values underestimated the true values by up to 40%. The adjusted ICP-MS data corrects for a 40% underestimate (i.e., measured value/0.6) and represents an upper bound of the true Ag^+ concentration. Error bars for the calculated concentrations represent predicted standard deviations based on variations in the total specimen area and the incubation time, error bars for the measured concentrations represent the standard deviation of experiments performed in triplicate, and error bars for the adjusted concentrations are the standard deviation of the adjusted triplicate samples.

The predicted concentrations obtained from the AFM results were fit with a pseudo-first-order kinetic model to approximate mass-based first-order rate constants for comparison with values found in the literature (see SI for details). The rate constants increased linearly between 0.01 and 0.10 d^{-1} over the 10−550 mM NaCl range. These first-order rate constants are lower than rate constants reported in previous studies on AgNP dissolution, which is contrary to expectations because the catalytic effect of NaCl is absent from the previous studies;[18−20] however, mass-based rate constants are not always comparable for surface-mediated reactions. For example, one study showed that three mass-based silver dissolution rate constants that varied by 5 orders of magnitude were all consistent with a surface recession rate of 2 nm/d.[17] Thus, reporting mass-based rate constants for AgNP dissolution may have little practical value. Interestingly, the 2 nm/d dissolution rate reported was for a pH 4 acetate buffer,[17] which is the same dissolution rate observed in this study for pH 7 and 550 mM NaCl. Given the accelerated dissolution of AgNPs at low pH,[18] this surface area normalized comparison is consistent with the observation that NaCl enhances AgNP dissolution rates.

Although our results and others indicate that chloride will catalyze AgNP dissolution, Liu and Hurt observed a slight inhibition of AgNP dissolution in seawater.[18] AgCl precipitation could have diminished Ag^+ release, but the authors' equilibrium calculations predicted that nearly 100% of dissolved silver would be present as soluble chloride complexes in their system. Their seawater matrix may have hindered their Ag^+ measurements, similar to what occurred with the ICP-MS analysis in this study, but the authors did not give any indication that such interference occurred. Another possibility is that some component of the seawater prevented NaCl-enhanced corrosion of the AgNPs. Importantly, Liu and Hurt observed that AgNPs aggregated in the seawater, but they concluded that neither ionic strength nor aggregation had a strong influence on the dissolution kinetics.[18] In this study, we have clearly demonstrated that NaCl enhances AgNP dissolution, and it is thus reasonable to conclude that AgNP aggregation in the samples studied by Liu and Hurt may have had a quenching effect similar in magnitude to the catalyzing influence of the high NaCl concentration in seawater. Past studies with iron oxides and galena have indicated the importance of aggregation state on nanomaterial dissolution rates.[23,24]

To further explore the hypothesis that aggregation impedes AgNP dissolution we offer alternate interpretations of previous results. Kittler et al. observed that poly(vinylpyrrolidone) (PVP)-coated AgNPs dissolved more rapidly than citrate-coated AgNPs, but no explanation for this result was given.[20] PVP stabilizes AgNPs against aggregation more effectively than citrate,[46] so the increased dissolution rate of PVP-coated AgNPs could be due to decreased aggregation. It has also been reported that AgNPs achieve a pseudoequilibrium that is dependent on the initial AgNP concentration and size, a hypothesis explained by citing the size-dependent thermodynamic properties of AgNPs,[19,20] and that mass-based AgNP dissolution rate constants decreased as the concentration of AgNPs increased.[18,19] Both these phenomena could be caused by the depletion of molecular oxygen and hydrogen ions;[18,20]

dx.doi.org/10.1021/es203475a | Environ. Sci. Technol. XXXX, XXX, XXX−XXX

however, this possibility does not appear to hold in at least one case where these trends are apparent.[19] Another interpretation is that aggregation and dissolution act as competing processes, both of which depend on initial nanoparticle concentration and size. At higher AgNP concentrations, more interparticle collisions lead to more rapid aggregation causing dissolution rate constants to decline. The pseudoequilibrium could be a function of how much Ag^+ was released before aggregation almost completely quenched the dissolution reaction. Of course, the degree of quenching is expected to depend on the aggregate size and structure. Large, dense aggregates would diminish exposed surface area and hinder mass transport of reactants to active sites more effectively than small, open aggregates.[23,26] Dissolution rate, solution chemistry, surface coating, concentration, and particle size and shape may all impact aggregation rate and aggregate size and structure;[19,50] therefore, the effects of aggregation on AgNP dissolution may be more pronounced in some situations than others.

Environmental Implications. Because NaCl is ubiquitous in natural waters, it will potentially have a strong influence on the environmental dissolution kinetics of AgNPs, particularly in saline waters and biological media. Laboratory investigations are often confounded by precipitation of AgCl at the high AgNP concentrations used in many studies.[45,51] Recognizing the possibility of AgCl precipitation, one research group excluded Cl^- from an otherwise realistic aqueous medium.[19] Thus, many laboratory studies may underestimate realistic AgNP dissolution rates. The experimental technique employed herein overcomes this dilemma by eliminating the potentially confounding use of high AgNP concentrations.

As discussed, aggregation may quench AgNP dissolution. High ionic strength can lead to rapid AgNP aggregation, but polymer coatings and adsorbed humic substances can provide added stability by an electrosteric mechanism.[46] AgNPs that are electrosterically stabilized may experience only slight aggregation in high ionic strength waters, so dissolution may govern AgNP fate in this scenario. Future efforts will focus on using NSL to investigate the effects of surface coating, size, and shape on AgNP dissolution under various environmental conditions in the absence of aggregation. Information obtained from these experiments is essential to understanding the interplay between dissolution and aggregation processes and the ultimate fate of AgNPs in the environment.

■ ASSOCIATED CONTENT

Supporting Information

Information about the silver digestion procedure, discussion regarding mathematical formulations of particle shape and silver concentrations, regression equations for predicting AgNP dissolution rates as a function of NaCl concentration, mass-based first-order dissolution rate constants, SEM images documenting NSL-produced AgNP aggregation, discussion of AFM lateral resolution issues, and XPS spectra. This information is available free of charge via the Internet at http://pubs.acs.org.

■ AUTHOR INFORMATION

Corresponding Author

*E-mail: pvikes@vt.edu; phone: 540-231-3568.

■ ACKNOWLEDGMENTS

This material is based upon work supported by the National Science Foundation (NSF) and the Environmental Protection Agency (EPA) under NSF Cooperative Agreement EF-0830093, Center for the Environmental Implications of NanoTechnology (CEINT). Any opinions, findings, conclusions or recommendations expressed in this material are those of the authors and do not necessarily reflect the views of the NSF or the EPA. This work has not been subjected to EPA review and no official endorsement should be inferred. We thank Dr. Jeffrey Parks and Jody Smiley for their assistance with ICP-MS and Dr. Jerry Hunter for his assistance with XPS. We thank Dr. Hans Robinson and Stefan Stoianov for their help with the NSL procedure. R.D.K. acknowledges the support of a Via M.S. fellowship from the Via Department of Civil and Environmental Engineering.

■ REFERENCES

(1) Fabrega, J.; Luoma, S. N.; Tyler, C. R.; Galloway, T. S.; Lead, J. R. Silver nanoparticles: Behaviour and effects in the aquatic environment. *Environ. Int.* **2011**, *37*, 517−531.

(2) Benn, T. M.; Westerhoff, P. Nanoparticle silver released into water from commercially available sock fabrics. *Environ. Sci. Technol.* **2008**, *42*, 4133−4139.

(3) Mueller, N. C.; Nowack, B. Exposure modeling of engineered nanoparticles in the environment. *Environ. Sci. Technol.* **2008**, *42*, 4447−4453.

(4) Geranio, L.; Heuberger, M.; Nowack, B. The behavior of silver nanotextiles during washing. *Environ. Sci. Technol.* **2009**, *43*, 8113−8118.

(5) Gottschalk, F.; Nowack, B. The release of engineered nanomaterials to the environment. *J. Environ. Monit.* **2011**, *13*, 1145−1155.

(6) Marambio-Jones, C.; Hoek, E. M. V. A review of the antibacterial effects of silver nanomaterials and potential implications for human health and the environment. *J. Nanopart. Res.* **2010**, *12*, 1531−1551.

(7) Morones, J. R.; Elechiguerra, J. L.; Camacho, A.; Holt, K.; Kouri, J. B.; Ramirez, J. T.; Yacaman, M. J. The bactericidal effect of silver nanoparticles. *Nanotechnology* **2005**, *16*, 2346−2353.

(8) Choi, O.; Hu, Z. Q. Size dependent and reactive oxygen species related nanosilver toxicity to nitrifying bacteria. *Environ. Sci. Technol.* **2008**, *42*, 4583−4588.

(9) Elechiguerra, J. L.; Burt, J. L.; Morones, J. R.; Camacho-Bragado, A.; Gao, X.; Lara, H. H.; Yacaman, M. J. Interaction of silver nanoparticles with HIV-1. *J. Nanobiotechnol.* **2005**, *3*, 6−15.

(10) Pal, S.; Tak, Y. K.; Song, J. M. Does the antibacterial activity of silver nanoparticles depend on the shape of the nanoparticle? A study of the gram-negative bacterium *Escherichia coli*. *Appl. Environ. Microbiol.* **2007**, *73*, 1712−1720.

(11) Kvitek, L.; Panacek, A.; Soukupova, J.; Kolar, M.; Vecerova, R.; Prucek, R.; Holecova, M.; Zboril, R. Effect of surfactants and polymers on stability and antibacterial activity of silver nanoparticles (NPs). *J. Phys. Chem. C* **2008**, *112*, 5825−5834.

(12) Lok, C.; Ho, C.; Chen, R.; He, Q.; Yu, W.; Sun, H.; Tam, P.; Chiu, J.; Che, C. Silver nanoparticles: Partial oxidation and antibacterial activities. *J. Biol. Inorg. Chem.* **2007**, *12*, 527−534.

(13) Gao, J.; Youn, S.; Hovsepyan, A.; Llaneza, V. L.; Wang, Y.; Bitton, G.; Bonzongo, J. C. J. Dispersion and toxicity of selected manufactured nanomaterials in natural river water samples: Effects of water chemical composition. *Environ. Sci. Technol.* **2009**, *43*, 3322−3328.

(14) Fabrega, J.; Fawcett, S. R.; Renshaw, J. C.; Lead, J. R. Silver nanoparticle impact on bacterial growth: Effect of pH, concentration, and organic matter. *Environ. Sci. Technol.* **2009**, *43*, 7285−7290.

(15) Sotiriou, G. A.; Pratsinis, S. E. Antibacterial activity of nanosilver ions and particles. *Environ. Sci. Technol.* **2010**, *44*, 5649−5654.

(16) Navarro, E.; Piccapietra, F.; Wagner, B.; Marconi, F.; Kaegi, R.; Odzak, N.; Sigg, L.; Behra, R. Toxicity of silver nanoparticles to *Chlamydomonas reinhardtii*. *Environ. Sci. Technol.* **2008**, *42*, 8959−8964.
(17) Liu, J.; Sonshine, D. A.; Shervani, S.; Hurt, R. H. Controlled release of biologically active silver from nanosilver surfaces. *ACS Nano* **2010**, *4*, 6903−6913.
(18) Liu, J.; Hurt, R. H. Ion release kinetics and particle persistence in aqueous nano-silver colloids. *Environ. Sci. Technol.* **2010**, *44*, 2169−2175.
(19) Zhang, W.; Yao, Y.; Sullivan, N.; Chen, Y. S. Modeling the primary size effects of citrate-coated silver nanoparticles on their ion release kinetics. *Environ. Sci. Technol.* **2011**, *45*, 4422−4428.
(20) Kittler, S.; Greulich, C.; Diendorf, J.; Koller, M.; Epple, M. Toxicity of silver nanoparticles increases during storage because of slow dissolution under release of silver ions. *Chem. Mater.* **2010**, *22*, 4548−4554.
(21) Levard, C. M.; Reinsch, B. C.; Michel, F. M.; Oumahi, C.; Lowry, G. V.; Brown, G. E. Sulfidation processes of PVP-coated silver nanoparticles in aqueous solution: Impact on dissolution rate. *Environ. Sci. Technol.* **2011**, *45*, 5260−5266.
(22) Vikesland, P. J.; Heathcock, A. M.; Rebodos, R. L.; Makus, K. E. Particle size and aggregation effects on magnetite reactivity toward carbon tetrachloride. *Environ. Sci. Technol.* **2007**, *41*, 5277−5283.
(23) Liu, J.; Aruguete, D. M.; Murayama, M.; Hochella, M. F. Influence of size and aggregation on the reactivity of an environmentally and industrially relevant nanomaterial (PbS). *Environ. Sci. Technol.* **2009**, *43*, 8178−8183.
(24) Rubasinghege, G.; Lentz, R. W.; Park, H.; Scherer, M. M.; Grassian, V. H. Nanorod dissolution quenched in the aggregated state. *Langmuir* **2010**, *26*, 1524−1527.
(25) Hotze, E. M.; Labille, J.; Alvarez, P.; Wiesner, M. R. Mechanisms of photochemistry and reactive oxygen production by fullerene suspensions in water. *Environ. Sci. Technol.* **2008**, *42*, 4175−4180.
(26) Hotze, E. M.; Bottero, J. Y.; Wiesner, M. R. Theoretical framework for nanoparticle reactivity as a function of aggregation state. *Langmuir* **2010**, *26*, 11170−11175.
(27) Haynes, C. L.; Van Duyne, R. P. Nanosphere lithography: A versatile nanofabrication tool for studies of size-dependent nanoparticle optics. *J. Phys. Chem. B* **2001**, *105*, 5599−5611.
(28) Haynes, C. L.; Mcfarland, A. D.; Smith, M. T.; Hulteen, J. C.; Van Duyne, R. P. Angle-resolved nanosphere lithography: Manipulation of nanoparticle size, shape, and interparticle spacing. *J. Phys. Chem. B* **2002**, *106*, 1898−1902.
(29) Hulteen, J. C.; Treichel, D. A.; Smith, M. T.; Duval, M. L.; Jensen, T. R.; Van Duyne, R. P. Nanosphere lithography: Size-tunable silver nanoparticle and surface cluster arrays. *J. Phys. Chem. B* **1999**, *103*, 3854−3863.
(30) Hulteen, J. C.; Van Duyne, R. P. Nanosphere lithography - A materials general fabrication process for periodic particle array surfaces. *J. Vac. Sci. Technol., A* **1995**, *13*, 1553−1558.
(31) Jensen, T. R.; Duval, M. L.; Kelly, K. L.; Lazarides, A. A.; Schatz, G. C.; Van Duyne, R. P. Nanosphere lithography: Effect of the external dielectric medium on the surface plasmon resonance spectrum of a periodic array of sliver nanoparticles. *J. Phys. Chem. B* **1999**, *103*, 9846−9853.
(32) Grabar, K. C.; Freeman, R. G.; Hommer, M. B.; Natan, M. J. Preparation and characterization of Au colloid monolayers. *Anal. Chem.* **1995**, *67*, 735−743.
(33) Chen, K.; Stoianov, S. V.; Bangerter, J.; Robinson, H. D. Restricted meniscus convective self-assembly. *J. Colloid Interface Sci.* **2010**, *344*, 315−320.
(34) Chen, K.; Durak, C.; Heflin, J. R.; Robinson, H. D. Plasmon-enhanced second-harmonic generation from ionic self-assembled multilayer films. *Nano Lett.* **2007**, *7*, 254−258.
(35) Markiewicz, P.; Goh, M. C. Atomic-force microscopy probe tip visualization and improvement of images using a simple deconvolution procedure. *Langmuir* **1994**, *10*, 5−7.
(36) Wiley, B.; Herricks, T.; Sun, Y.; Xia, Y. Polyol synthesis of silver nanoparticles: Use of chloride and oxygen to promote the formation of single-crystal, truncated cubes and tetrahedrons. *Nano Lett.* **2004**, *4*, 1733−1739.
(37) Yang, J.; Zhang, Q.; Lee, J. Y.; Too, H. Dissolution−recrystallization mechanism for the conversion of silver nanospheres to triangular nanoplates. *J. Colloid Interface Sci.* **2007**, *308*, 157−161.
(38) Ho, C.; Yau, S.; Lok, C.; So, M.; Che, C. Oxidative dissolution of silver nanoparticles by biologically relevant oxidants: A kinetic and mechanistic study. *Chem. Asian J.* **2010**, *5*, 285−293.
(39) Gottschalk, F.; Sonderer, T.; Scholz, R. W.; Nowack, B. Modeled environmental concentrations of engineered nanomaterials (TiO_2, ZnO, Ag, CNT, fullerenes) for different regions. *Environ. Sci. Technol.* **2009**, *43*, 9216−9222.
(40) Blaser, S. A.; Scheringer, M.; Macleod, M.; Hungerbühler, K. Estimation of cumulative aquatic exposure and risk due to silver: Contribution of nano-functionalized plastics and textiles. *Sci. Total Environ.* **2008**, *390*, 396−409.
(41) Zhang, X.; Hicks, E. M.; Zhao, J.; Schatz, G. C.; Van Duyne, R. P. Electrochemical tuning of silver nanoparticles fabricated by nanosphere lithography. *Nano Lett.* **2005**, *5*, 1503−1507.
(42) Plieth, W. J. Electrochemical properties of small clusters of metal atoms and their role in surface enhanced Raman scattering. *J. Phys. Chem.* **1982**, *86*, 3166−3170.
(43) Redmond, P. L.; Hallock, A. J.; Brus, L. E. Electrochemical Ostwald ripening of colloidal Ag particles on conductive substrates. *Nano Lett.* **2005**, *5*, 131−135.
(44) Yanina, S. V.; Rosso, K. M. Linked reactivity at mineral-water interfaces through bulk crystal conduction. *Science* **2008**, *320*, 218−222.
(45) Li, X.; Lenhart, J. J.; Walker, H. W. Dissolution-accompanied aggregation kinetics of silver nanoparticles. *Langmuir* **2010**, *26*, 16690−16698.
(46) Huynh, K. A.; Chen, K. L. Aggregation kinetics of citrate and polyvinylpyrrolidone coated silver nanoparticles in monovalent and divalent electrolyte solutions. *Environ. Sci. Technol.* **2011**, *45*, 5564−5571.
(47) Henglein, A.; Linnert, T.; Mulvaney, P. Reduction of Ag^+ in aqueous polyanion solution: Some properties and reactions of long-lived oligomeric silver clusters and metallic silver particles. *Ber. Bunsen-Ges. Phys. Chem* **1990**, *94*, 1449−1457.
(48) Henglein, A.; Mulvaney, P.; Linnert, T. Chemistry of Ag_n, aggregates in aqueous solution: Non-metallic oligomeric clusters and metallic particles. *Faraday Discuss.* **1991**, *92*, 31−44.
(49) Bloxham, M. J.; Hill, S. J.; Worsfold, P. J. Determination of trace-metals in sea-water and the online removal of matrix interferences by flow-injection with inductively-coupled plasma-mass spectrometric detection. *J. Anal. At. Spectrom* **1994**, *9*, 935−938.
(50) Hotze, E. M.; Phenrat, T.; Lowry, G. V. Nanoparticle aggregation: Challenges to understanding transport and reactivity in the environment. *J. Environ. Qual.* **2010**, *39*, 1909−1924.
(51) Scheckel, K. G.; Luxton, T. P.; El Badawy, A. M.; Impellitteri, C. A.; Tolaymat, T. M. Synchrotron speciation of silver and zinc oxide nanoparticles aged in a kaolin suspension. *Environ. Sci. Technol.* **2010**, *44*, 1307−1312.